Kinetic Energy Budgets of a Subtropical Squall Line Determined from TAMEX Dual-Doppler Measurements

YEONG-JER LIN AND HSI SHEN*

Department of Earth and Atmospheric Sciences, Saint Louis University, St. Louis, Missouri

ROBERT W. PASKEN

Department of Mathematics, Parks College of Saint Louis University, Cahokia, Illinois

(Manuscript received 30 May 1990, in final form 6 September 1990)

ABSTRACT

Dual-Doppler data collected during the Taiwan Area Mesoscale Experiment (TAMEX) are used to study the kinetic energy balance of a subtropical squall line over the Taiwan Straits. Values of each term in the kinetic energy budget equation are assessed from the Doppler-derived winds and retrieved thermodynamic variables using 1-km grid spacing in all three directions. The budget domain has horizontal dimensions of 23×40 km^2, covering the convective region of the squall line. Results show that vertical totals of the horizontal generation and total buoyancy production terms act as a source of kinetic energy, while vertical totals of dissipation and vertical generation provide the main sinks. The horizontal flux divergence (convergence) of kinetic energy is nearly balanced by the vertical flux convergence (divergence) at most levels. The computed tendencies agree well with the observed tendencies in the lower and upper layers. The vertical total of kinetic energy change is negative for both the observed and computed values, showing the decrease of total kinetic energy of the squall system as it approached the west coast of Taiwan.

1. Introduction

Kinetic energy studies of the meso-β-scale storm environment were reported in studies by Kung and Tsui (1975), Tsui and Kung (1977), and Fuelberg and Printy (1984). Results showed that the convective environment was energetically very active when compared to the entire analyzed domain. The convective environment was characterized by large generation and dissipation of kinetic energy at the jet stream level. Magnitudes of energy transformations in the convective environment were significantly larger and their effects were more discernible than at the synoptic scale.

There are very few observational studies in the literature that describe the effects of convection on its meso-γ-scale environment. Using the dual-Doppler data collected during JAWS (Joint Airport Weather Studies), Lin and Coover (1988) conducted a kinetic energy analysis of a microburst-producing thunderstorm with 0.5-km grid spacing. Results showed that vertical totals of the horizontal generation and horizontal flux divergence terms acted as a source of kinetic energy, while a vertical total of dissipation was a sink. Magnitudes of the horizontal and vertical flux divergence terms for the storm scale were one order of magnitude greater than those for the storm environment in the lower and middle layers.

Recently, the kinematic, dynamic, and thermodynamic structures of a subtropical squall line over the Taiwan Straits have been studied by Wang et al. (1990) and Lin et al. (1990) using dual-Doppler data. This squall line occurred on 17 May 1987 within the network of Taiwan Area Mesoscale Experiment (TAMEX) in northern Taiwan. It is typical of those squall lines that approach Taiwan. Findings showed that many properties of the subtropical squall line are similar to those for a tropical squall line, but are different from a midlatitude squall line. The depth of the subtropical squall line was lower than 12 km, the maximum updraft was less than 14 m s^{-1}, the maximum reflectivity was smaller than 50 dBZ, and the line speed was 16.5 m s^{-1} from 250°.

This study is an extension of the studies by Wang et al. (1990) and Lin et al. (1990), employing the same dataset at three analysis times in intervals of 3 min. The purpose is to investigate the kinetic energy balance of a subtropical squall line as it approached the west coast of Taiwan. Kinetic energy budgets are assessed over the horizontal domain of 23×40 km^2 covering the convective region. The important physical processes contributing to the kinetic energy budget are investigated. The goal is to gain a better understanding of a fast-moving subtropical squall line over the ocean.

Corresponding author address: Dr. Yeong-Jer Lin, Department of Earth and Atmospheric Sciences, St. Louis University, 3507 Laclede Avenue, St. Louis, MO 63103.

2. Data and methodology

As described in studies by Wang et al. (1990) and Lin et al. (1990), dual-Doppler data from the CP-4 and TOGA radars at 0040, 0043, and 0046 LST (local standard time) 17 May 1987 were used to investigate the structure and internal dynamics of a subtropical squall line. These data were objectively analyzed to produce a detailed wind field at 10 analysis levels in the vertical ranging from 0.3 to 8.8 km. The horizontal and vertical grid spacing was 1 km except for the lowest two levels, where δz was chosen to be 0.5 km. Vertical velocities were computed from the anelastic continuity equation by integrating downward with variational adjustment.

Once the three-dimensional wind field was derived, fields of deviation perturbation pressure and virtual temperature were retrieved from the Doppler-derived winds using the three momentum equations (e.g., Gal-Chen 1978; Lin et al. 1986; Parsons et al. 1987; etc.). The tendency terms in thermodynamic retrieval were determined from dual-Doppler observations at two successive scans. The retrieved field was subjected to momentum checking (E_r) to determine the level of confidence. Low values of E_r, say $E_r \leq 0.35$, indicate that the agreement is good between the retrieved (best fit) horizontal pressure gradients and the pressure gradients derived from the individual momentum equations (including all terms). Values of E_r obtained in this study range from 0.29 to 0.40 with a volume mean of approximately 0.33.

Following the study by Lin and Coover (1988), the kinetic energy equation for a nonhydrostatic system can be written as

$$\underbrace{\left\langle \frac{\partial \rho_o K_3}{\partial t} \right\rangle}_{\text{LTK}} = \underbrace{-\langle \nabla_h \cdot (\rho_o K_3 \mathbf{V}_h) \rangle}_{\text{HFD}} \underbrace{- \left\langle \frac{\partial \rho_o K_3 w}{\partial z} \right\rangle}_{\text{VFD}} - \underbrace{\langle \mathbf{V}_h \cdot \nabla_h P' \rangle}_{\text{HGE}} \underbrace{- \left\langle w \frac{\partial P'}{\partial z} \right\rangle}_{\text{VGE}} + \underbrace{\left\langle \rho_o g w \left(\frac{T'_v}{T_{vo}} - q_l \right) \right\rangle}_{\text{BUP}} + \underbrace{\langle \rho_o \mathbf{V} \cdot \mathbf{F} \rangle}_{\text{FDI}}, \quad (1)$$

where $\langle (\quad) \rangle = (1/\text{area}) \iint (\quad) dxdy$, $K_3 = (u^2 + v^2 + w^2)/2$ is the total kinetic energy per unit mass, the subscript o represents the environmental mean, the prime denotes the deviation from the environmental mean, and the other symbols have their conventional meanings. Terms on the right-hand side of (1) represent the horizontal flux divergence (HFD), the vertical flux divergence (VFD), the horizontal generation (HGE), the vertical generation (VGE), the total buoyancy production (BUP), and the frictional dissipation (FDI) of kinetic energy, respectively.

As shown by Lin and Coover (1988), the vertical generation term (VGE) can be approximated by

$$-\left\langle w \frac{\partial P'}{\partial z} \right\rangle = -\left\langle w \frac{\partial P'_d}{\partial z} \right\rangle - \langle w \rangle \frac{\partial \langle P' \rangle}{\partial z} \approx -\left\langle w \frac{\partial P'_d}{\partial z} \right\rangle. \quad (2)$$

Similarly, the thermal buoyancy term in term BUP can be approximated by

$$\frac{\rho_o g}{T_{vo}} \langle w T'_v \rangle = \frac{\rho_o g}{T_{vo}} (\langle w T'_{vd} \rangle + \langle w \rangle \langle T'_v \rangle) \approx \frac{\rho_o g}{T_{vo}} \langle w T'_{vd} \rangle, \quad (3)$$

where P'_d and T'_{vd} represent deviation perturbation pressure and virtual temperature, respectively. These quantities are defined as $P'_d \equiv P' - \langle P' \rangle$ and $T'_{vd} \equiv T'_v - \langle T'_v \rangle$ (Gal-Chen 1978), where $\langle \quad \rangle$ is the height-dependent area mean averaged over a 23×40 km^2 horizontal domain.

The validity of (2) and (3) depends on the area mean of vertical velocity $\langle w \rangle$ going to zero or remaining very small. For a typical convective storm with updrafts and downdrafts in coexistence, the $\langle w \rangle$ value averaged over the whole horizontal domain will be much smaller than magnitudes of the convective updrafts and downdrafts at a given height. Our calculation has confirmed that the maximum value of $\langle w \rangle$ is only about 1 m s^{-1} at 4 km and becomes much smaller in the layers above and below (see Fig. 12 in Lin et al. 1990), whereas the extreme values of w range from -6 to 13 m s^{-1} for most convective cells embedded within the squall line. To the best of our estimate, the accuracy of (2) and (3) is within 20% for the case being investigated.

As depicted in the study by Gal-Chen (1978), the thermodynamic retrieval method recovers fields of P'_d and T'_{vd} from a detailed wind field and reflectivity information using the three momentum equations. The viability of the method, to a large extent, depends on the accuracy of wind and reflectivity fields. The P'_d field is retrieved from the Doppler-derived winds using the two horizontal momentum equations, while the T'_{vd} field is obtained from the buoyancy equation using the derived three-dimensional winds and pressures. In addition, dynamically retrieved buoyancy is not constrained by latent heating/cooling since the thermodynamic energy equation is not used. As a result, in some updraft regions, the retrieved T'_{vd} values may not be in total agreement with latent heating. For these reasons, the term BUP is less accurate than the other terms in (1). This must be taken into account when the budget results are interpreted.

In an attempt to show the relationships between w and T'_{vd}, a linear correlation coefficient r between the two quantities is calculated at each analysis level

within the domain of interest. Results show that values of r range from 0.41 to 0.72 with an average of 0.55 at heights below 7 km. The best values ($r > 0.63$) occur in the layer between 1.5 and 4.5 km, where upward motion dominates in the convective region. These findings suggest that the retrieved temperatures correlate well with the convective updrafts/downdrafts in most regions in the lower and midtroposphere and are plausible in terms of latent heating/cooling. Accordingly, some useful information can be extracted from the retrieved thermodynamic variables for the budget study. In the upper troposphere ($z > 7$ km), however, the agreement between the retrieved temperature field and vertical velocity is relatively poor. Values of r are smaller than 0.4, showing a little correlation between T'_{vd} and w. This finding is expected since the Doppler-derived winds and radar reflectivity are subject to larger errors in the upper troposphere than those in the lower and midtroposphere. As a result, caution must be exercised to interpret the buoyancy field at levels above 7 km, which is less accurate than that at levels below. This buoyancy field does not appear plausible in terms of latent heating/cooling.

3. Discussion of results

a. *Squall-line characteristics*

Some structural features of the subtropical squall line under investigation were detailed in studies by Wang et al. (1990) and Lin et al. (1990). At the times of analysis (0040, 0043, and 0046 LST), the leading edge of the squall line was located approximately 10–20 km west of the west coast of Taiwan. For illustration, the field of storm-relative wind with reflectivity contours superimposed for 2.75 km at 0043 LST is shown in Fig. 1. The box in the figure signifies the horizontal domain used for budget calculation. A pronounced line of horizontal convergence is evident, especially in the northern portion of the leading edge (see the heavy dashed line in Fig. 1). Its position is coincident with the highest reflectivity regions. However, the agreement farther south is not as good. On the east side of the convergence line, storm-relative winds are predominantly from the southeast, resulting in a front-to-rear flow in the direction normal to the leading edge. On the other hand, the southwest winds prevail in the areas west of the convergence line. These winds produce a flow from the back toward the leading edge. This rear-to-front flow from the midtroposphere plays an important role in initiation and maintenance of the convective downdrafts.

Figure 2 displays the reflectivity field with vertical velocities superimposed for 2.75 km. In the figure, upward motion > 3 m s^{-1} is shaded, while downward motion < -3 m s^{-1} is hatched. There are many cells embedded within the squall line. The old (main) cells are approximately located in the central portion of Fig. 2 ($-22 < x < -12$ km) with the new cells to their east

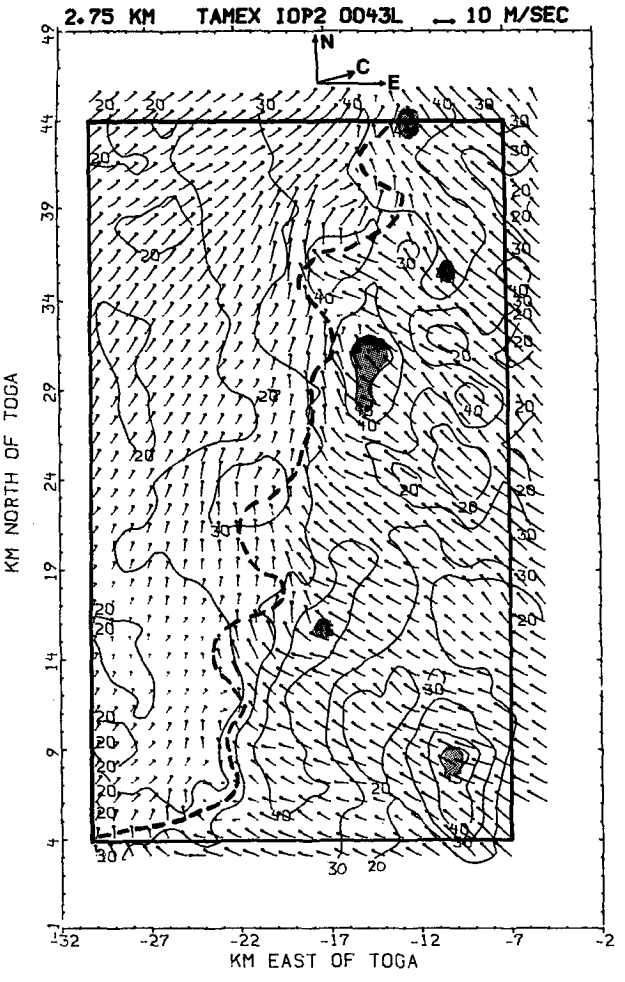

FIG. 1. Horizontal storm-relative winds with reflectivity Z contours superimposed for 2.75 km at 0043 LST 17 May 1987. Distances are in kilometers from the TOGA radar. Contour interval for Z is 10 dBZ with $Z > 45$ dBZ shaded. The box signifies the horizontal domain of 23×40 km^2. The heavy dashed line shows the convergence line at this level. East (E) and north (N) directions and storm motion (C) are indicated.

($x > -12$ km). Note that upward motion matches well with the high reflectivity region at this level. Convective downdrafts (hatched) occur between the old and new cells and behind the old cells. The leading edge is oriented almost in a north–south direction.

Results from the studies by Wang et al. (1990) and Lin et al. (1990) showed that many structural features of a subtropical squall line were similar to those of a fast-moving tropical squall line. A low-level jet (LLJ) provided the necessary strong shear at low levels. On the front side of the squall line, front-to-rear flow prevailed at all levels with maxima at lower and upper levels and a minimum at middle levels. A shallow layer (1–3 km) of the rear-to-front flow, entering from the backside of the convective region, transported cooler midtropospheric air into the lower layer. Part of the negatively buoyant air from the rear continued to move

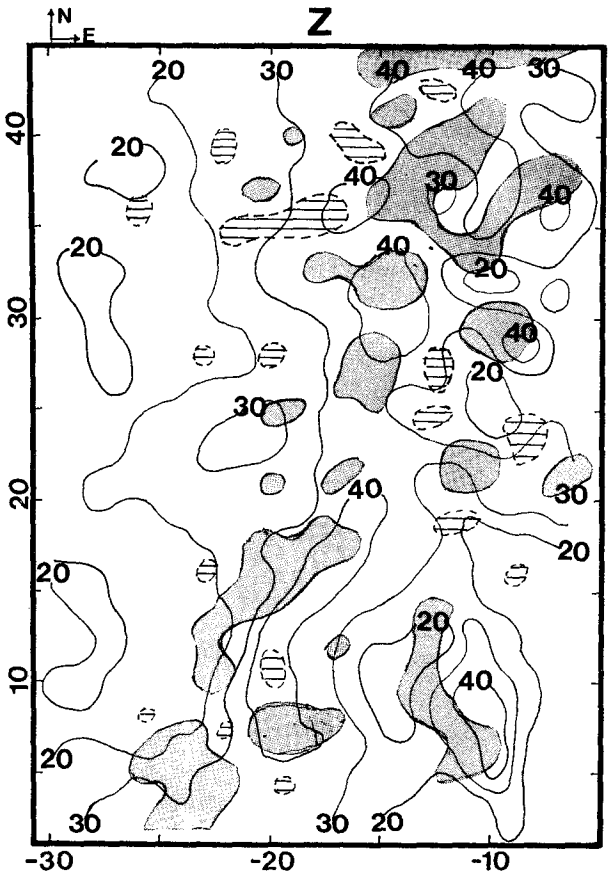

FIG. 2. Horizontal variations of radar reflectivity Z and vertical velocity w for 2.75 km at 0043 LST 17 May 1987. Contour interval for Z is 10 dBZ. Values of $w > 3$ m s^{-1} are shaded, while areas with $w < -3$ m s^{-1} are hatched. East (E) and north (N) directions are indicated. Distances are in kilometers from the TOGA radar.

forward, colliding with the advancing high-θ_e air in the boundary layer. As a result, new convective cells formed ahead of the old cells, thereby prolonging the lifetime of the squall line. The retrieved fields of pressure and temperature perturbations agreed well with the updraft–downdraft structure. In general, high pressure formed below the saturated, cool convective downdrafts behind the gust front, and low pressure developed underneath the convective updraft near and above the gust front. Relative warming occurred in updrafts due to the latent heat release by condensation, while relative cooling prevailed in downdrafts due to evaporative cooling. The momentum budget calculation revealed that the horizontal and vertical flux convergences/divergences of horizontal momentum by the mean and eddy motions are the major contributor to maintain the mean momentum.

b. Horizontal variations of kinetic energy

Budgets of the total kinetic energy per unit volume for each level were computed from (1) over a 23 × 40 km^2 horizontal domain (see the box in Fig. 1) at each analysis time. As noted earlier, three volume scans of dual-Doppler data centered at 0040, 0043, and 0046 LST 17 May were considered in this study. The tendency terms were determined from the Doppler-derived winds for each level at two successive scans. Results obtained for each analysis time were then compared to those at another time. Findings reveal that the overall kinetic energy budgets are quite comparable from one analysis time to the other. These findings are reasonable since the structure of the subtropical squall line did not change much at the time span of 6 min as depicted in studies by Wang et al. (1990) and Lin et al. (1990). In the following, only the results at 0043 LST are presented for discussion. The tendency terms were evaluated from the data at 0040 and 0046 LST using the centered differencing scheme.

Figure 3 shows horizontal distributions of HFD and VFD at 2.75 km. The area of integration for these terms is one grid square (1 × 1 km^2). It will be shown later that these two terms are dominant over the other terms at most levels in the budget equation. For the horizontal flux term (Fig. 3a), large positive values (convergence) of HFD occur in the high-reflectivity regions along the convergence line seen in Fig. 1. Similarly, positive values of HFD are also found in the new cells to the east of the old cells. Conversely, negative values of HFD (divergence) occur between the new and old cells and behind the old cells. The opposite is true for term VFD (Fig. 3b), with flux divergence (negative) in the convective updrafts and flux convergence (positive) in the convective downdrafts. Values of HFD and VFD have the same order of magnitude but opposite signs throughout the domain, showing the near balance between the two terms.

The horizontal distribution of thermal buoyancy (BUO) is depicted in Fig. 4. It is seen that positive values of BUO dominate over the whole horizontal domain. As mentioned earlier, a positive value of BUO occurs when the warm air rises and the cool air descends. Examination of Figs. 2 and 4 reveals that the maxima of BUO are located in the convective updrafts (see the shaded areas in Fig. 2), showing the positive correlation between temperature perturbations and upward motion. A correlation coefficient r at this level is 0.72. In other words, a gain of kinetic energy at this level is largely due to the ascent of warmer air in updrafts.

In an effort to further show the relationships between the buoyancy field and vertical velocity in the lower, middle, and upper layers of the squall system, horizontal variations of Z, w, P'_d, and T'_{vd} along the east–west cross section 36 km north of TOGA are presented in Fig. 5. The cross section passes through one of the convective cells, located near $-18 < x < -12$ km, with a reflectivity maximum in excess of 40 dBZ. At 0.73 km, downward motion dominates in the area west of the maximum reflectivity ($x < -17$ km). The retrieved T'_{vd} field shows that the temperature deficit ($T'_{vd} < 0$) coincides with downward motion. This cool, near-sat-

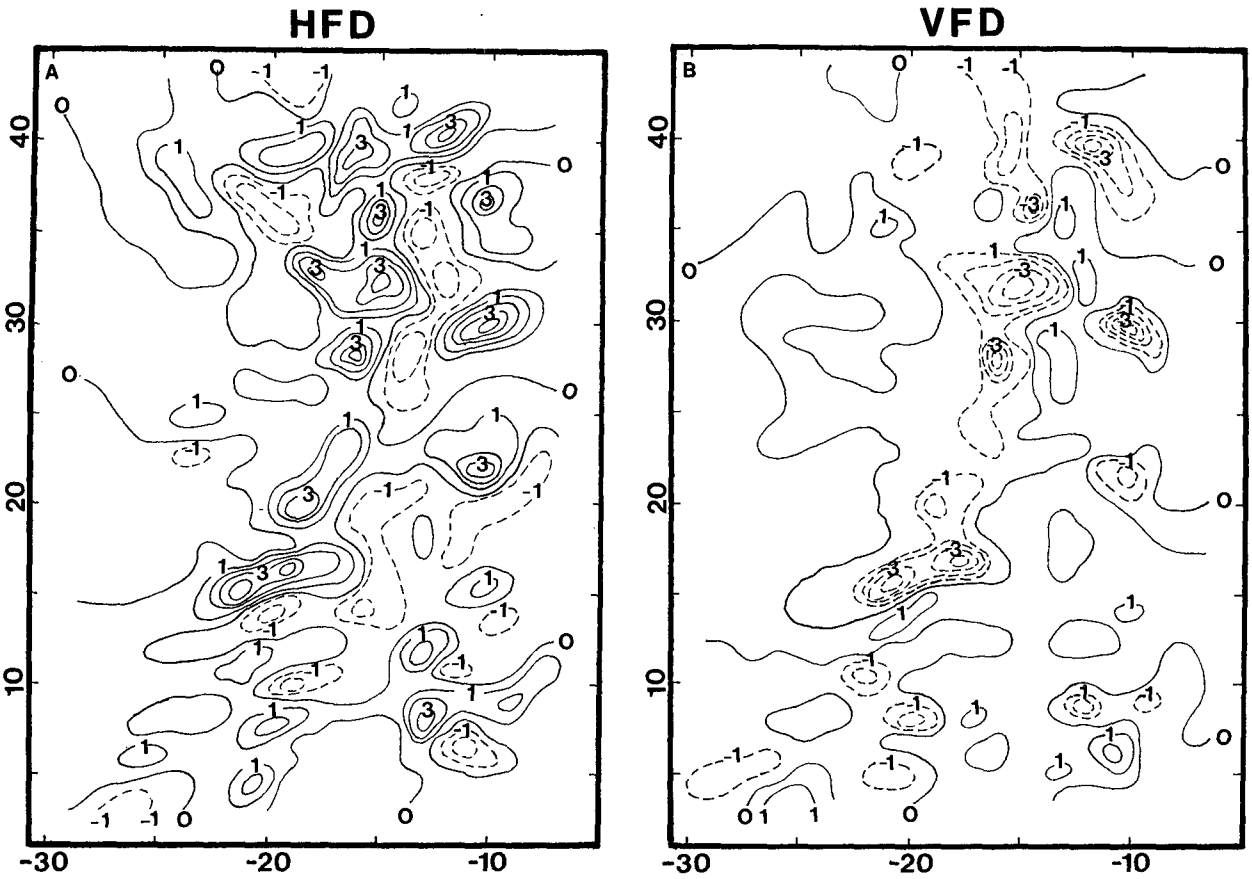

FIG. 3. Horizontal distributions of the (a) horizontal flux divergence (HFD) and (b) vertical flux divergence (VFD) of kinetic energy for 2.75 km at 0043 LST 17 May 1987. Distances are in kilometers from the TOGA radar. Units are in 10^{-1} W m^{-3}. Contour interval is 1 $\times 10^{-1}$ W m^{-3} with negative values dashed.

urated air is the product of the convective downdraft, located on the west side of the convective updraft, and results in a cold surface outflow (Wang et al. 1990; Lin et al. 1990). In the updraft region ($-16 < x < -12$ km), a positive value of 1° reflects high-θ_e air rising from below. Note that the gust front is located near -15 km. At the gust front, the high-θ_e environmental air from the east is lifted, feeding the updraft. Behind the gust front ($x < -15$ km), the air is relatively cool (-0.5°C), indicative of the cool-saturated convective downdraft. A temperature contrast is evident across the gust front. At 3.73 km, the convective downdraft ($-19 < x < -16$ km) is in the high-reflectivity core, indicating that negative buoyancy of the downdraft air is increased due to precipitation loading. To the west of the convective updrafts, there is a weak updraft ($-24 < x < -19$ km), which is accompanied by another downdraft to its west. In general, the temperature excess matches well with upward motion and the temperature deficit corresponds to downward motion. In a similar manner, the T'_{vd} field is correlated with vertical velocity at 6.74 km. Inspection of Fig. 5 further reveals that centers of the maximum and minimum temperature are located about 1 km to the east of the updraft and downdraft maxima, respectively, in agreement with that reported in studies by Hane and Ray (1985) and Lin et al. (1986).

Figure 6 shows the east–west cross section 16 km north of TOGA. As in Fig. 5, the intimate relationship between vertical velocity and temperature is apparent at all three levels. In general, the temperature excess occurs in the convective updraft, while the temperature deficit develops in the convective downdraft. The maximum temperature excess is 2°C with a minimum of -1.5°C at 3.73 km. Somewhat smaller values are observed in the upper and lower layers. It is worth noting that the correlation coefficients between T'_{vd} and w over a 23 $\times$ 40 km^2 horizontal domain are 0.55, 0.63, and 0.41 for 0.73, 3.73, and 6.74 km, respectively. These results imply that the retrieved buoyancy field is plausible in terms of latent heating/cooling at 0.73- and 3.73-km levels, but is less plausible at 6.74 km and higher up. This point will be further discussed later.

c. *Kinetic energy budget*

Budgets of the total kinetic energy, per unit volume, were calculated from (1) by integrating over a 23 $\times$ 40

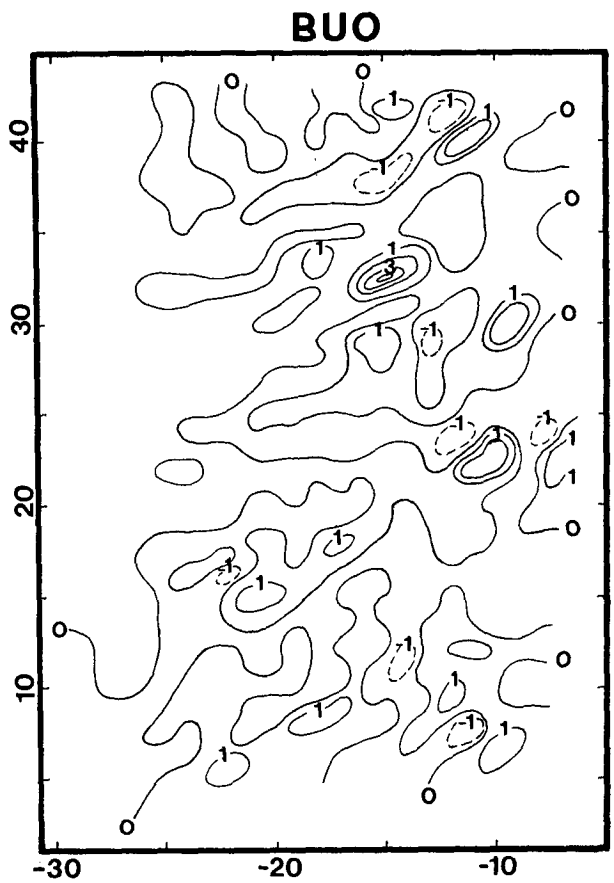

FIG. 4. As in Fig. 3, except for thermal buoyancy production (BUO) of kinetic energy.

km^2 horizontal domain at each level. Figure 7 shows vertical profiles of terms HFD and VFD. A positive (negative) value indicates the flux convergence (divergence). Note that the term HFD is positive at levels below 3.5 km and is negative aloft, in agreement with the field of convergence and divergence. In contrast, the term VFD gives flux divergence of kinetic energy in the layer below 3 km with flux convergence higher up. Note that the term HFD is nearly in balance with the term VFD at most levels. The total flux term (TFD) is the sum of these two terms (see the dotted line in Fig. 7). It shows a net gain of kinetic energy in the layers below 4 km with a net loss above. The mean vertical transport of kinetic energy, $\langle \rho_o K_3 w \rangle$, is presented in Fig. 8. It shows how the total kinetic energy is transferred from one level to another. Notice that an upward transport dominates throughout the troposphere with the maximum ($\approx$30 W m^{-2}) occurring in the 2–3-km layer. This feature implies that the total kinetic energy, averaged over the convective region of interest, is consistently transferred upward due to an organized convection within the line.

Vertical variations of the terms HGE, VGE, and BUP are displayed in Fig. 9. Note that magnitudes of all three terms are much smaller than those of HFD and VFD at most levels (Fig. 7). The horizontal generation term (HGE) provides a sink of kinetic energy at levels below 3 km with a source above. This result is opposite to that for a microburst-producing storm (Lin and Coover 1988). The positive contribution of HGE occurs when the wind blows from high pressure to low pressure, while HGE becomes negative when the wind blows from low pressure to high pressure. The negative value of HGE below 3 km is largely due to the horizontal pressure gradient, which is predominantly from the west to east at the leading edge of the squall line, in association with the southeast inflow (Lin et al. 1990). In contrast, the direction of horizontal pressure gradients is approximately from east to west in the middle and upper layers, resulting in positive values of HGE. On the other hand, the vertical gen-

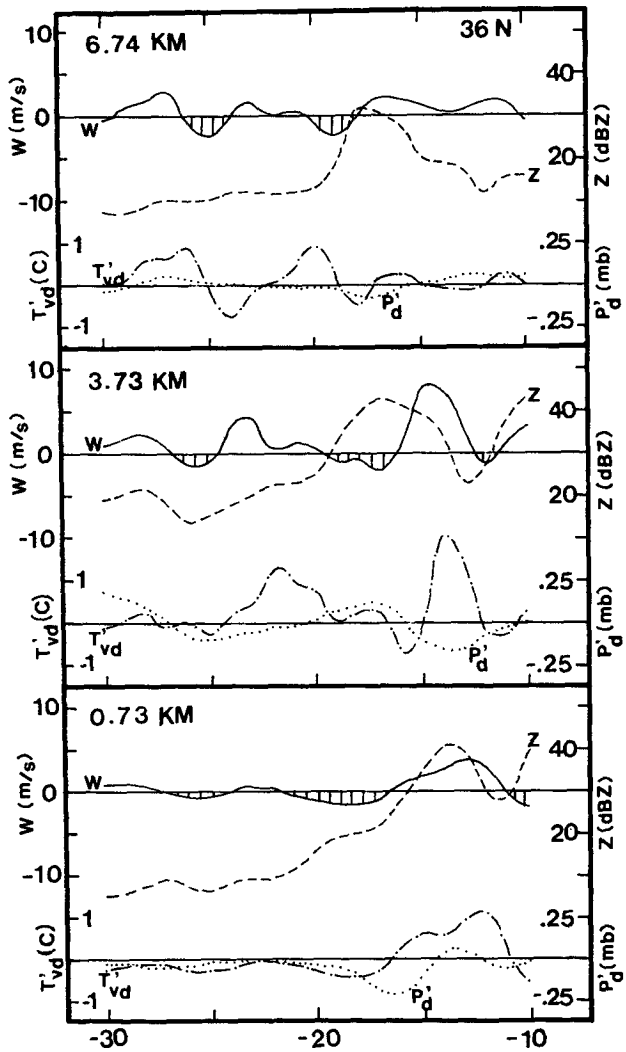

FIG. 5. Horizontal variations of reflectivity Z, vertical velocity w, deviation perturbation pressure P'_d, and deviation virtual temperature T'_{vd} at 0.73, 3.73, and 6.74 km. The east–west cross section is located 36 km north of TOGA.

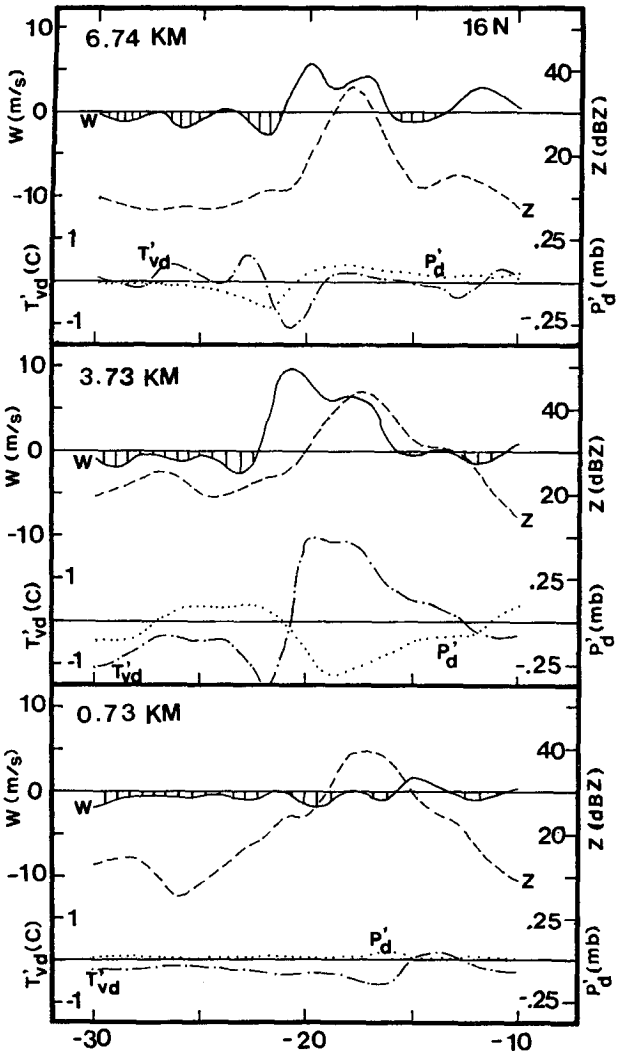

FIG. 6. As in Fig. 5, except for a cross section 16 km north of TOGA.

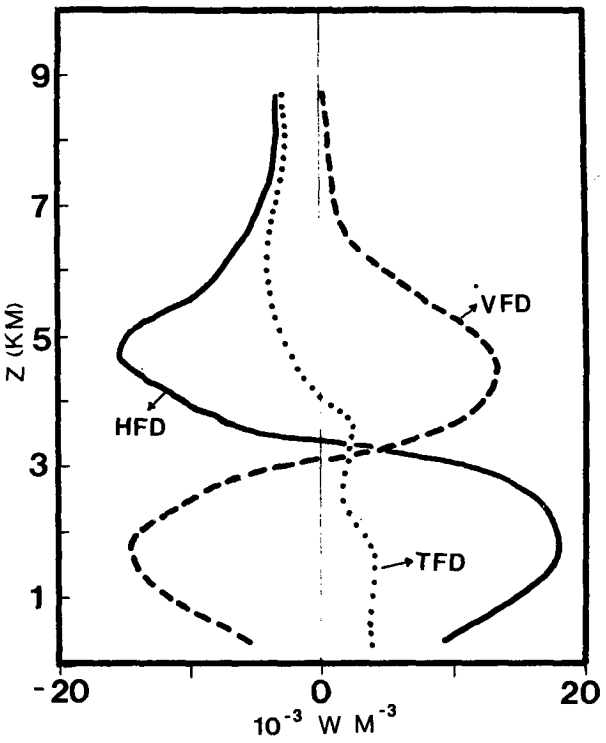

FIG. 7. Vertical profiles of the horizontal flux divergence (HFD), vertical flux divergence (VFD), and total flux divergence (TFD) of kinetic energy. Units are in 10^{-3} W m^{-3}.

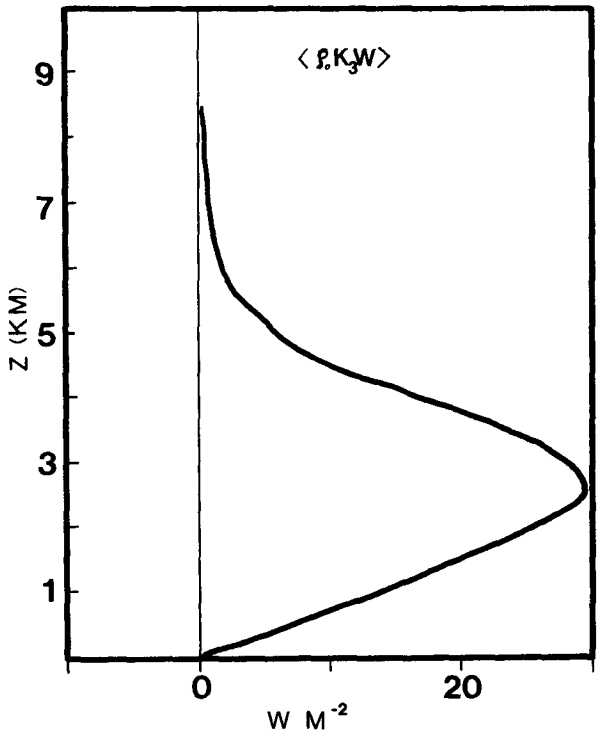

FIG. 8. The vertical distribution of mean vertical kinetic energy transport $\langle \rho_o K_3 w \rangle$. Units are in watts per square meter (W m^{-2}).

eration term (VGE) has negative values in the layer between 1 and 6 km with positive values above and below that layer.

In Fig. 9, the kinetic energy production due to the total buoyancy (BUP) is also plotted (dotted line). This term is composed of the contributions of thermal buoyancy (BUO) and precipitation loading. The latter normally has the negative contribution to BUP, while the former can either be positive or negative. A source of kinetic energy from the buoyancy production occurs when the warm air rises and the cold air descends, while a sink forms when the warm air is forced to descend and the cold air is lifted upward. Notice that values of BUP are positive in the layer below 4 km. In this layer, the warm air ascends within the convective updrafts (BUP > 0), due to the latent heat release by condensation, resulting in a gain of kinetic energy over that layer. In the same layer, the cool air descends within the convective downdrafts, due to evaporative

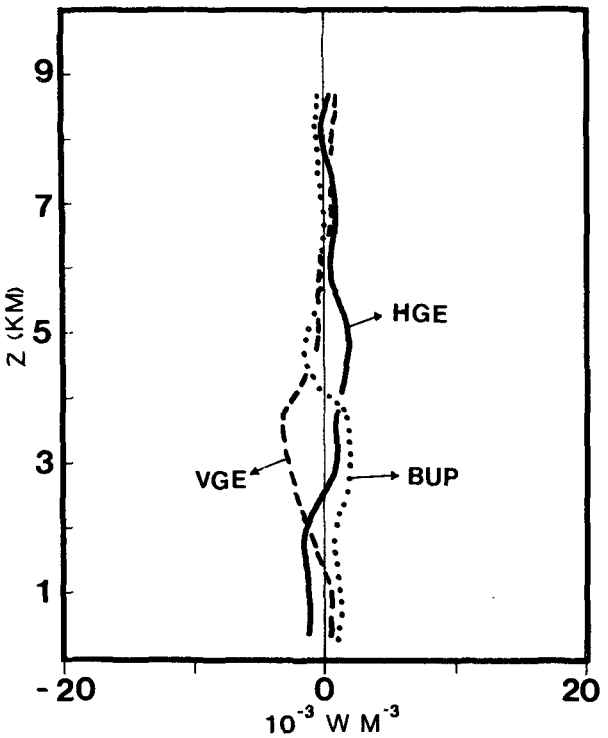

FIG. 9. As in Fig. 7, except for the horizontal generation (HGE), vertical generation (VGE), and total buoyancy production (BUP) of kinetic energy.

cooling and rain loading, resulting in a positive generation of BUP. Values of BUP become negative in the layer above 4 km due, in part, to the combined effects of thermal buoyancy and precipitation loading. Note that precipitation loading overcomes thermal buoyancy in the midtroposphere (4–6 km), resulting in a negative value of BUP there. It must be pointed out that values of BUP become less reliable at heights above 7 km (see section 2). Examination of Fig. 9 reveals that terms VGE and BUP have the same order of magnitude but opposite signs at most levels. This finding is consistent with that reported in the study by Lin and Coover (1988).

The frictional dissipation term (FDI) in this study was calculated from the parameterization scheme of Klemp and Wilhelmson (1978). This approach is different from that of Tsui and Kung (1977) and Fuelberg and Printy (1984). In these two studies, emphasis was placed on the storm's environment using the conventional upper-air data. The dissipation term was not calculated directly; instead, it was estimated from the kinetic energy budget equation as a residual.

Figure 10 shows the vertical profile of term FDI. The magnitude of FDI is relatively small when compared with the other terms in (1). Values of FDI are negative at all levels, showing a sink of kinetic energy due to frictional dissipation.

The computed tendency LTK is obtained from (1) as a residual. This term should equal the sum of the net generation/dissipation inside the mesoscale domain and the net flux through the lateral analysis domain boundaries. It contains not only the information of physical processes and actual storm evolutions contributing to a gain/loss of kinetic energy, but also errors in data sampling and numerical computation. These errors include the uncertainty in u, v, w, P'_d, and T'_{vd} estimates, the parameterization errors in friction and precipitation loading, the truncation errors, etc. For these reasons, term LTK should be carefully interpreted in a qualitative manner. It is worth noting that integration over the horizontal domain is a powerful remover of noise. Consequently, the impact of random errors on the computation of each term in (1) is largely reduced. From Figs. 7, 9, and 10, we found that magnitudes of HFD and VFD are about one order of magnitude larger than the other terms in (1) at most levels. These two terms are determined directly from the Doppler-derived winds and, thus, are more accurate than the generation, buoyancy production, and frictional dissipation terms in the budget equation. These findings suggest that some useful information can still be extracted from the tendency term (LTK) concerning the time change of total kinetic energy within the subtropical squall line.

In Fig. 10, the computed tendency of kinetic energy (LTK) and the observed tendency (OBS) are also plotted. Note that term LTK has positive values in a shallow layer below 2 km and negative values aloft. This

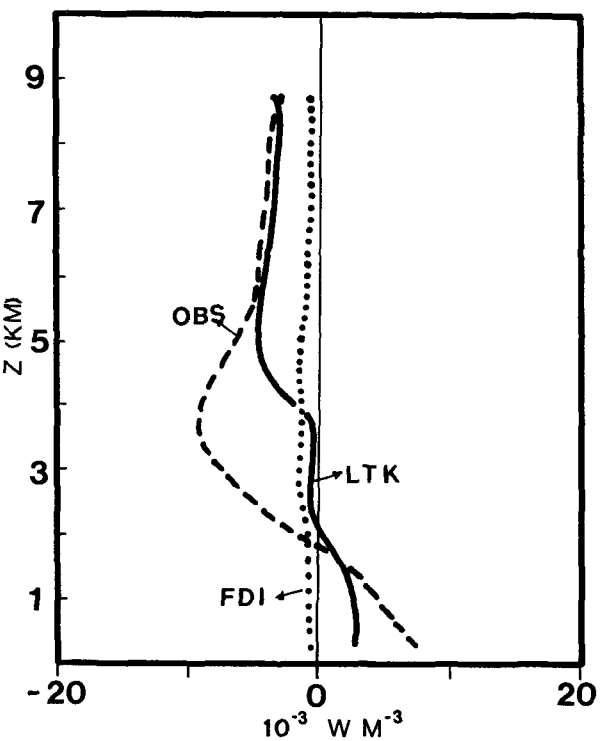

FIG. 10. Vertical profiles of the frictional dissipation (FDI), local time change of kinetic energy (LTK), and observed tendency of kinetic energy (OBS). Units are in 10^{-3} W m^{-3}.

implies that the kinetic energy of the system is increasing with time in the lower layer and is decreasing with time in the middle and upper layers. Magnitudes of LTK are generally small compared with terms HFD and VFD (Fig. 7) at most levels. The observed tendency also exhibits a net gain of kinetic energy in the lower layer ($z < 2$ km) and a net loss at levels above 2 km. A comparison between the term LTK and the observation (OBS) reveals that these two terms are in agreement in the upper and lower layers. In the middle layer ($2 < z < 5$ km), however, the computed values are much smaller than the observed values. The disagreement in the middle layer may be attributed, in part, to the errors mentioned previously.

d. *Vertical totals of kinetic energy*

Table 1 presents budgets of the total kinetic energy averaged over a 23×40 km^2 horizontal domain (see the box in Fig. 1) and integrated over a depth of 1 km. Note that term FDI has negative values (sink) at all levels. The magnitude is generally smaller than the flux terms at most levels. Two flux terms (HFD and VFD) have much larger values in the layers below 6 km. These two terms are nearly in balance at every level. As a result, the sum of these two terms, that is, the total flux divergence (TFD), becomes relatively small when compared to the individual flux term. Similar to the flux terms, the vertical generation term (VGE) and the total buoyancy production term (BUP) are of the same order of magnitude but opposite signs at most levels. The computed tendency (LTK) shows the increase of kinetic energy with time in the layer from the surface to 3 km and the decrease in the middle and upper layers. This finding implies that the squall line had gradually reduced its total kinetic energy with time as it approached the west coast of Taiwan, showing the effect of topography on convection. This point will be further investigated in our future study using additional datasets for the same storm system. Like the computed tendencies, the observed tendencies (OBS) also exhibit the decrease of the total kinetic energy at most levels except in the lowest layer ($z < 2$ km). The computed tendencies appear to agree with the observations at most levels except in the layer between 2 and 5 km.

The vertical total in Table 1 presents the total budget of each term from the surface to 9 km near the storm top. Note that the frictional dissipation term acts as a sink (-8.1 W m^{-2}) of kinetic energy. Similarly, the terms HFD (-1.2 W m^{-2}), VFD (-0.1 W m^{-2}), and VGE (-7.1 W m^{-2}) are also sinks of kinetic energy. On the other hand, sources of kinetic energy come from the terms HGE (1.4 W m^{-2}) and BUP (2.9 W m^{-2}). Vertical totals for LTK and OBS are -12.1 and -30.3 W m^{-2}, respectively, showing the decrease of total kinetic energy within the convective system at the times of analysis.

In the kinetic energy study of a microburst-producing storm in Colorado, Lin and Coover (1988) found that the frictional dissipation term provides a sink (-13.5 W m^{-2}) of kinetic energy, while the horizontal flux divergence term (10.2 W m^{-2}) and the horizontal generation term (5.1 W m^{-2}) act as a source. Another source of kinetic energy (6.0 W m^{-2}) comes from the total buoyancy production, which is offset by the loss due to the term VGE (-5.5 W m^{-2}). Comparison between their study and this study shows some similarities and differences in kinetic energy budgets. The most significant difference occurs in the horizontal flux divergence term (HFD). Ours is a weak sink and theirs is a strong source of kinetic energy. Beside this, the vertical totals of the remaining terms in the budget equation are quite comparable between the two studies. It must be pointed out that the study by Lin and Coover (1988) used the horizontal domain of 10×10 km^2 with 0.5-km grid spacing to include the most area of a microburst-producing storm in Colorado. In contrast, this study has the horizontal domain of 23×40 km^2 with 1-km grid spacing, covering only the northern portion of the whole squall line in northern Taiwan. Ours is organized oceanic convection in the subtropical latitudes with abundant moisture in the environment, while theirs was a midlatitude thunderstorm in the relatively dry environment over the high land. Ours is a

TABLE 1. Kinetic energy budgets, averaged over a 23×40 km^2 horizontal domain and integrated over a depth of 1 km, at 0043 LST 17 May 1987. Units are in watts per square meter (W m^{-2}). The vertical totals from the study by Lin and Coover (1988), abbreviated LC, are shown at the bottom.

Layer (km)	HFD	VFD	TFD	HGE	VGE	BUP	FDI	LTK	OBS
8–9	−3.07	0.16	−2.91	0.14	0.31	−0.33	−0.32	−3.11	−3.12
7–8	−3.64	0.59	−3.05	0.16	0.20	−0.16	−0.48	−3.33	−3.90
6–7	−6.07	2.28	−3.79	0.71	0.06	−0.19	−0.66	−3.87	−4.69
5–6	−10.66	7.24	−3.42	0.73	−0.65	−0.70	−1.06	−5.10	−5.61
4–5	−13.30	12.73	−0.57	1.59	−1.34	−0.83	−1.28	−2.43	−8.26
3–4	−4.63	6.28	1.65	0.80	−3.15	1.91	−1.32	−0.11	−8.85
2–3	11.78	−9.46	2.32	0.12	−2.20	1.57	−1.54	0.27	−4.47
1–2	17.23	−12.66	4.57	−1.55	−0.57	0.78	−0.82	2.41	2.20
sfc–1	11.21	−7.27	3.94	−1.32	0.27	0.88	−0.62	3.15	6.44
Vertical total	−1.15	−0.11	−1.26	1.38	−7.07	2.93	−8.10	−12.12	−30.26
LC	10.19	0.07	10.26	5.05	−5.46	6.03	−13.53	2.35	

squall line embedded within the mesoscale convective system (MCS) with many old and new cells in the convective region. Conversely, theirs was a local convective system with a huge convective downdraft associated with the rain shaft, which produced a microburst in the boundary layer ($z \leq 1$ km). Indeed, there are some differences in structure and internal dynamics between the two systems being investigated. These must be taken into account when the results from the two studies are interpreted.

4. Conclusions

The Doppler-derived winds and the retrieved thermodynamic variables at three analysis times were used to study the kinetic energy balance of a subtropical squall line over the Taiwan Straits. Results show that: 1) the horizontal and vertical flux divergence terms are nearly in balance, having the same order of magnitude but opposite signs at most levels; 2) the total kinetic energy is transported upward throughout the troposphere due to the organized convective updrafts; 3) the horizontal generation and total buoyancy production terms act as a source of kinetic energy with dissipation as the main sink; 4) the computed tendencies of kinetic energy agree well with the observed tendencies in the lower and upper troposphere; and 5) the vertical total of kinetic energy change is negative, showing the decrease of kinetic energy within the squall system as it approached the west coast of Taiwan.

Acknowledgments. The authors wish to express their appreciation to those scientists, technicians, and staff members who participated in the TAMEX project. We would like to thank the National Center for Atmospheric Research (NCAR) for providing Doppler data and technical assistance. Special thanks go to the National Science Council of the Republic of China and the National Science Foundation for supporting the field experiment. Discussions with T. C. Chen Wang and S. C. Lin of National Central University are appreciated. Suggestions from two anonymous reviewers have helped improve the manuscript. This work has been supported by the Atmospheric Science Division, National Science Foundation, under NSF Grant ATM-8609150.

REFERENCES

Fuelberg, H. E., and M. F. Printy, 1984: A kinetic energy analysis of the meso-β-scale severe storm environment. *J. Atmos. Sci.*, **41,** 3212–3226.

Gal-Chen, T., 1978: A method for the initialization of the anelastic equations: Implications for matching models with observations. *Mon. Wea. Rev.*, **106,** 587–606.

Hane, C. E., and P. S. Ray, 1985: Pressure and buoyancy fields derived from Doppler radar in a tornadic thunderstorm. *J. Atmos. Sci.*, **42,** 18–35.

Klemp, J. B., and R. B. Wilhelmson, 1978: The simulation of three-dimensional convective storm dynamics. *J. Atmos. Sci.*, **35,** 1070–1096.

Kung, E. C., and T. L. Tsui, 1975: Subsynoptic-scale kinetic energy balance in the storm area. *J. Atmos. Sci.*, **32,** 729–740.

Lin, Y. J., and J. A. Coover, 1988: A kinetic energy analysis of a microburst-producing thunderstorm based on JAWS dual-Doppler data. *J. Atmos. Sci.*, **45,** 2764–2771.

——, T. C. Wang and J. H. Lin, 1986: Pressure and temperature perturbations within a squall-line thunderstorm derived from SESAME dual-Doppler data. *J. Atmos. Sci.*, **43,** 2302–2327.

——, ——, R. W. Pasken, H. Shen and Z. S. Deng, 1990: Characteristics of a subtropical squall line determined from TAMEX dual-Doppler data. Part II: Dynamic and thermodynamic structures and momentum budgets. *J. Atmos. Sci.*, **47,** 2382–2399.

Parsons, D. B., C. G. Mohr and T. Gal-Chen, 1987: A severe frontal rain band. Part III: Derived thermodynamic structure. *J. Atmos. Sci.*, **44,** 1615–1631.

Tsui, T. L., and E. C. Kung, 1977: Subsynoptic-scale energy transformations in various severe storm situations. *J. Atmos. Sci.*, **34,** 98–110.

Wang, T. C., Y. J. Lin, R. W. Pasken and H. Shen, 1990: Characteristics of a subtropical squall line determined from TAMEX dual-Doppler data. Part I: Kinematic structure. *J. Atmos. Sci.*, **47,** 2357–2381.